Progress In Electromagnetics Research M, Vol. 103, 185–196, 2021

Improving Electromagnetic Compatibility Performance of Narrowband-IoT SiP Module

Haiyan Sun[1, 2], Ting Zhou[1], Shoukun Huang[1], Jicong Zhao[1, 2, *], Zhilong Zhang[3], and Xiaoyong Miao[3]

Abstract—A package-board co-design method was applied for a Narrowband Internet of Things (NB-IoT) SiP module. The electromagnetic interference (EMI) generated by the module was studied by improving the transmission quality of radio frequency (RF) signal. The SiP models of the initial design and the optimized design were simulated separately to show that the optimized design significantly increased effective transmission power of the RF signal and suppressed near-field electromagnetic radiation intensity to a certain extent. In addition, the optimized design model was verified by measurement. The measured results show good agreement with the simulated ones and demonstrate that the package-board co-design method can improve the electromagnetic compatibility (EMC) of NB-IoT applications.

1. INTRODUCTION

The SiP technology can miniaturize RF transceiver system and improve the performance and stability of the entire system. However, the increasing capacities and shrinking dimensions of SiP package will lead to a complex electromagnetic environment [1–9]. Hence, the EMI caused by the complex electromagnetic environment inside a SiP model has become a serious problem. If the EMI cannot be effectively suppressed, it will not only influence the performance of the module itself, but also cause interference to the entire electronic system. Some methods to restrain the EMI have been studied, but most of them focus on the electromagnetic shielding outside the package. A shielded metal lid was traditionally used to block EMI radiation from device to device. Furthermore, conformal shielding will be a more effective method to decrease the EMI, because it has a smaller size and a lighter weight than a shielding cover [10–19]. Some novel shielding structures were applied to packages based on conformal shielding technology [20, 21]. In addition, the designed BVA wire bonding structure is also a good way to improve SiP integration and electrical performance [22, 23]. Although the above-mentioned EMI suppression methods are more conducive to meeting the measurement standard of radiation emission, they will increase the cost of a SiP module. If EMI can be restricted to a certain extent in the initial stage of package model design, it will definitely reduce the cost of solving EMI problem in the later stage.

It is known that EMI can be reduced by improving the signal transmission quality. Some different methods have been studied to improve the quality of signal transmission in different package types [24–30], but a quantitative analysis of generated electromagnetic radiation has rarely been performed. Therefore, it is necessary to study the EMI generated under an actual operating condition of SiP module from the perspective of signal transmission.

Received 5 April 2021, Accepted 23 June 2021, Scheduled 20 July 2021

* Corresponding author: Jicong Zhao (jczhao@ntu.edu.cn).

[1] School of Information Science and Technology, Nantong University, Nantong, China. [2] State Key Laboratory of Transducer Technology, Shanghai, China. [3] Tongfu Microelectronics Co., Ltd, Nantong, China.

In order to suppress EMI to a certain extent during the design stage, a package-board co-design method is adopted in this paper to effectively and reasonably design the RF channel that actually operates in the NB-IoT SiP module. The electromagnetic radiation generated by the SiP module was studied quantitatively by improving the transmission quality of RF signal. The SiP models of the initial design and optimized design were simulated separately, and their simulation results of S-parameter and electromagnetic radiation were compared and analyzed. Furthermore, the optimized SiP module was manufactured for near-field radiation measurement. The measured results of near-field radiation not only verified the correctness of the simulation modeling, but also indicated that the EMI generated by the optimized NB-IoT SiP module was suppressed to a certain extent successfully.

2. PACKAGE-BOARD CO-DESIGN OPTIMIZATION METHOD

An RF circuit system with the best performance is designed by using RF components with ideal interconnection. At the same time, the parasitic effects caused by interconnection structures are also added to the original ideal RF circuit. Figure 1 shows the S-parameter comparison results for the RF signal circuit with and without ideal interconnection. In order to evaluate the performance easily, the magnitude of -1 dB is considered as criterion associated with insertion loss (S_{21}), and the magnitude of -20 dB is considered as criterion associated with return loss (S_{11}). From Figure 1, the performance of

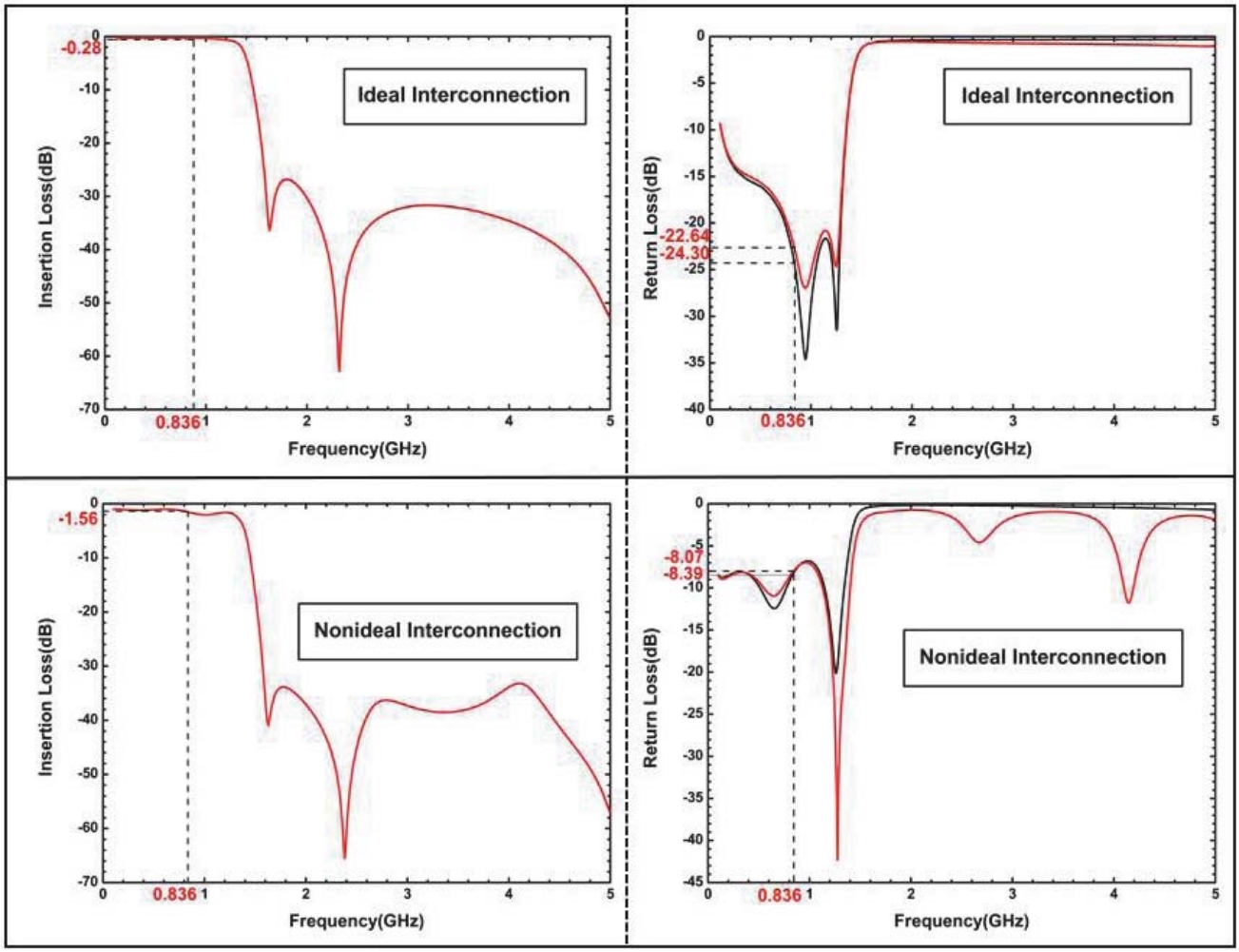

Figure 1. S-parameter comparison results for a same RF signal circuit with and without ideal interconnection structure.

ideal connection measured for S_{21} and S_{11} is -0.28 dB and -22.64 dB at 836 MHz, respectively, while the performance of nonideal connection measured for S_{21} and S_{11} deteriorates to -1.58 dB and -8.07 dB at 836 MHz. It can be seen that a better transmission quality is obtained with ideal interconnection at the operating frequency. However, the ideal interconnection structure does not exist in reality; therefore, it is necessary to optimize the nonideal connection structure to improve the transmission performance of RF signal.

It is well known that signal reflection will be produced when a transmission line is affected by a discontinuous impedance, such as a shunt capacitance or a series inductance. And the reflection amplitude of individual effect is greater than the combined reflection amplitude because the capacitance and inductance have opposite polarities. A negative reflection is generated when the discontinuous impedance is lower than the characteristic impedance Z_0 of transmission line. On the contrary, a positive reflection is produced.

Firstly, a discontinuous impedance structure is formed between the pads of two adjacent components and the transmission line connecting the two components in RF channel of SiP module. Its equivalent circuit is demonstrated in Figure 2.

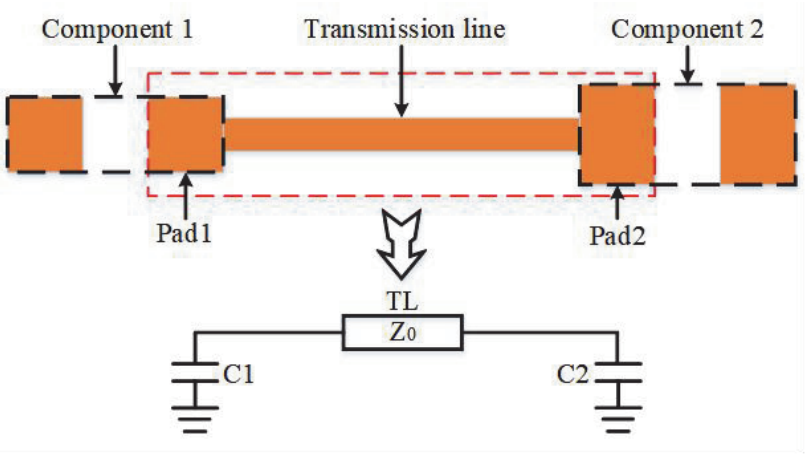

Figure 2. Equivalent circuit of component pads connection in RF channel.

A simple comparison circuit, as shown in Figure 3, was designed to effectively analyze and optimize this discontinuous impedance structure. Due to the different sizes of pads, some appropriate circuit constants were selected for simulation analysis.

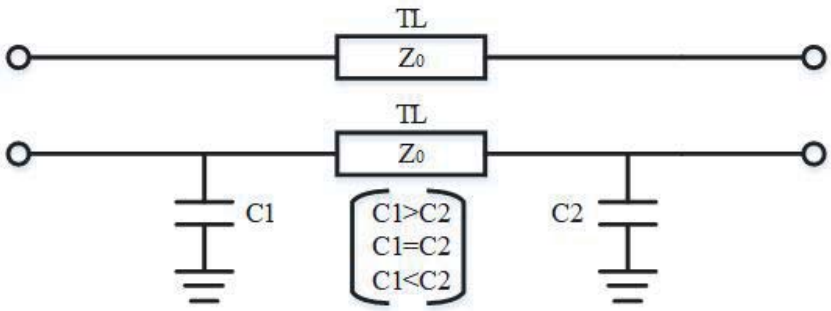

Figure 3. Designed equivalent comparison circuits. Appropriate circuit constants are selected for simple simulation verification.

The frequency responses of different capacitor combinations are shown in Figure 4. Therefore, the dielectric material, distance from the pads to the adjacent reference layer, and pad size are some crucial factors that affect the capacitance value. The discontinuous impedance of pads structure can be effectively improved by adopting these methods.

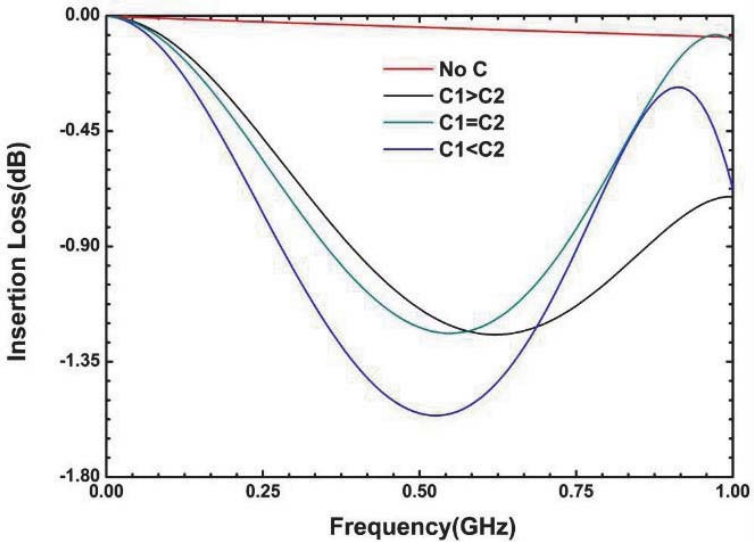

Figure 4. S_{21} of equivalent comparison circuits.

Additionally, via plays a very significant role in the SiP module, which is mainly used to connect the same signal between different signal layers, but it is also one of the discontinuous impedance structures in RF channel. Figure 5 illustrates the equivalent circuit model of a via structure in SiP module. It is known from the following simple calculation in Equation (1) of impedance Z_d that the via impedance can be controlled by changing the values of L and C.

$$Z_d = \sqrt{\frac{L}{C}} \tag{1}$$

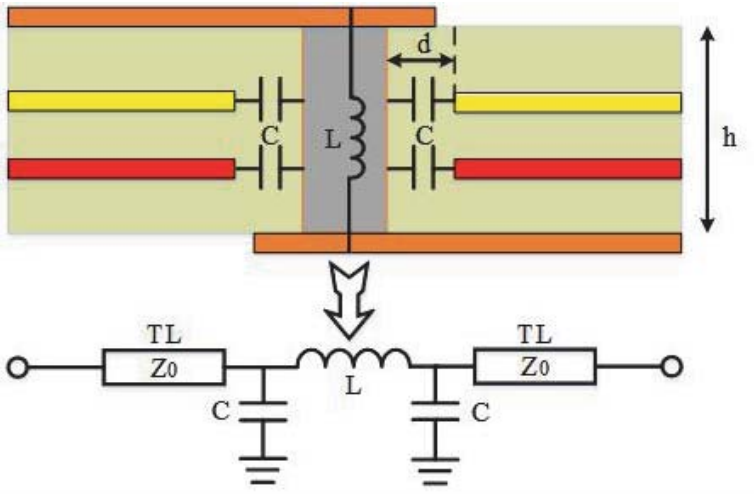

Figure 5. Equivalent circuit model of via structure.

Based on feasible and reliable manufacturing technology, shortening the physical length h of the via can improve the problem of discontinuous impedance, because the inductance and capacitance will be reduced in accordance with the proportion of via reduction at the same time. However, the discontinuous impendence cannot be completely eliminated, because the via cannot be fabricated sufficiently small. Furthermore, the distance d between the via and inner reference planes is reasonably designed to be a more effective method.

When the anti-pad radius is increased, the reduction of mutual-inductance makes the equivalent inductance increase, but the increase of distance d causes the equivalent capacitance to decrease, and they have the same factor α. In this case, the via impedance can be expressed as shown in Equation (2). It is easy to find from Equation (3) that if the anti-pad radius is reasonably designed, there will be a factor $\alpha = Z_0/Z_d$ such that the via impedance is equal to Z_0.

$$Z_{d'} = \sqrt{\frac{L \cdot \alpha}{C \cdot 1/\alpha}} = \alpha\sqrt{\frac{L}{C}} \tag{2}$$

$$Z_{d'} = \alpha\sqrt{\frac{L}{C}} = \alpha Z_d \overset{\alpha=\frac{Z_0}{Z_d}}{\longrightarrow} Z_{d'} = Z_0 \tag{3}$$

3. INITIAL NB-IOT PACKAGE-BOARD COLLABORATIVE MODELING AND SIMULATION

3.1. Initial NB-IoT Package-Board Collaborative Modeling

A system-level circuit is integrated in the NB-IoT module, which mainly includes a Hi2115 SoC processor chip for LPWAN communication, four RF signal channels, etc. An RF signal channel mainly includes a power amplifier, a filter, an RF switch, and some passive components, as shown in Figure 6. The entire system-level NB-IoT circuit is packaged in a Land Grid Array (LGA) package with 52 pins.

A test board for realizing co-simulation is modeled on a four-layer substrate. According to the test standard IEC61967-3 of IC EMC, almost all components of peripheral circuits are placed on the top

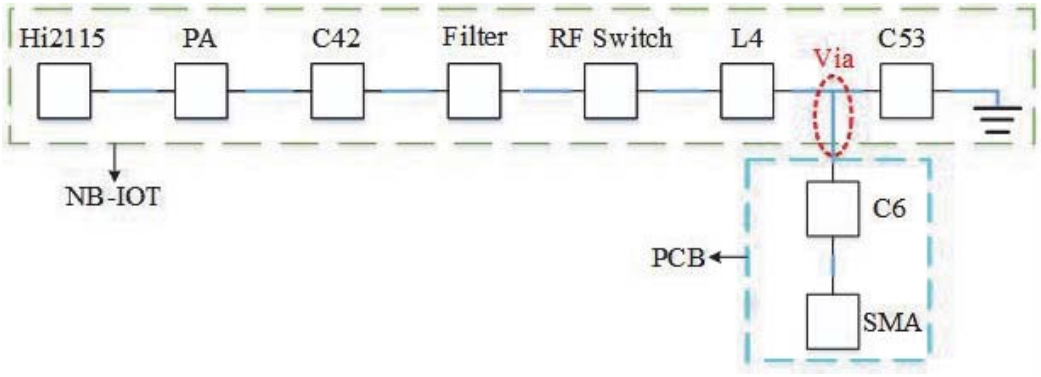

Figure 6. Output channel of the RF signal.

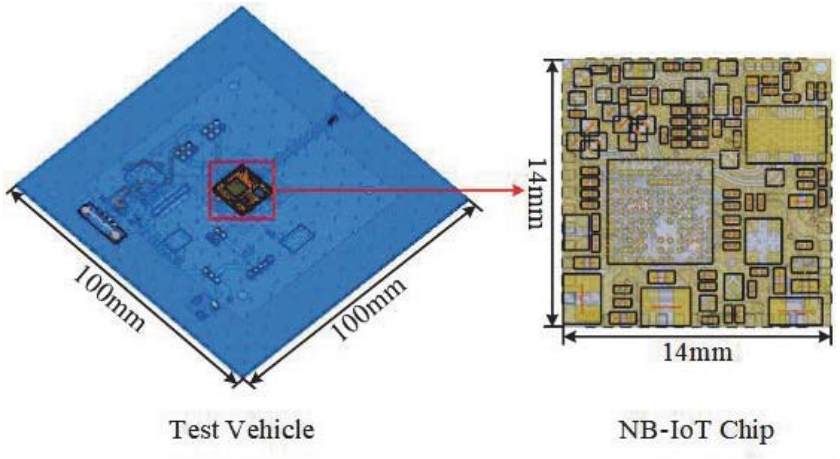

Figure 7. Package-board co-design model of NB-IoT module.

layer of the test board, and only the NB-IoT module is installed in the middle of the bottom layer. The whole simulation model is shown in Figure 7, where the size of the LGA package is 14 mm (length) × 14 mm (width) × 1.85 mm (height), and the test board is 100 mm(length) × 100 mm (width) × 1.5 mm (height).

3.2. Initial NB-IoT Collaborative Simulation and Results Analysis

S-parameter models were added to corresponding components of the RF channel to perform S-parameter simulation with frequency sweep from 0.1 GHz to 5 GHz. S-parameter reflects the correlation between transmitted power and reflected power from the perspective of energy transmission. Figure 8 shows the S-parameter simulation results. At the operating frequency of 836 MHz, S_{21} is −1.56 dB, and S_{11} is −8.39 dB.

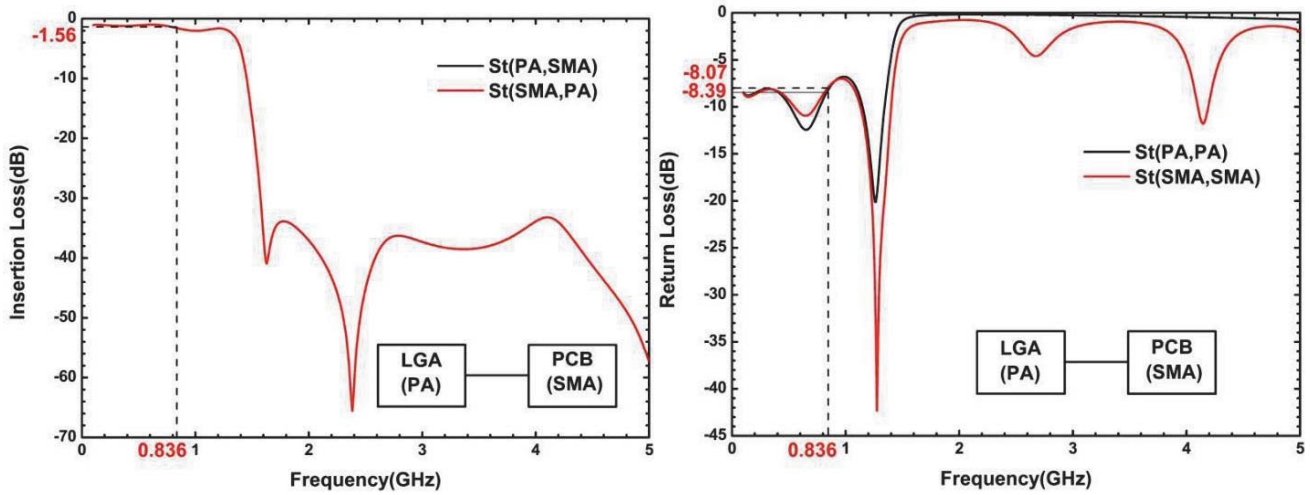

Figure 8. S-parameter simulation results of the initial design sweep from 0.1 GHz to 5 GHz. (a) S_{21} and (b) S_{11}.

However, the S-parameters indicate that the RF signal has great loss during transmission. Furthermore, the corresponding time-domain simulation result is shown in Figure 9. It can be seen that the signal amplitude of the receive port (red line) is significantly lower than the driver port (black line) in the initial design model, indicating that there is indeed a large energy loss in the process of signal transmission.

It is well known that the lost energy will be manifested by means of heat, electromagnetic radiation, etc. The electromagnetic radiation will interfere with other signals. In addition, an excessive EMI will cause chip to fail the EMC test standard. So it is necessary to study the electromagnetic radiation of the NB-IoT module working under the initial design model. A radiation observation plane is located at 3 mm directly above the LGA package, and its size is the same as the package. The near-field radiation intensity is quantified by an electric field (E-field) intensity and a magnetic field (H-field) intensity, as shown in Figure 10. The simulation results indicate that the radiation energy is mainly concentrated near the driver port. The maximums of E-field and H-field intensity are 1.062E+01 V/m and 2.007E-02 A/m, respectively.

4. PACKAGE-BOARD COLLABORATIVE OPTIMIZATION FOR NB-IOT MODULE

In order to study the effects of improving signal transmission quality on the electromagnetic radiation, the package-board co-design methods proposed in the second part are applied to the initial design model. The stack-up adjustment, dielectric material selection, and size design can be selected to control

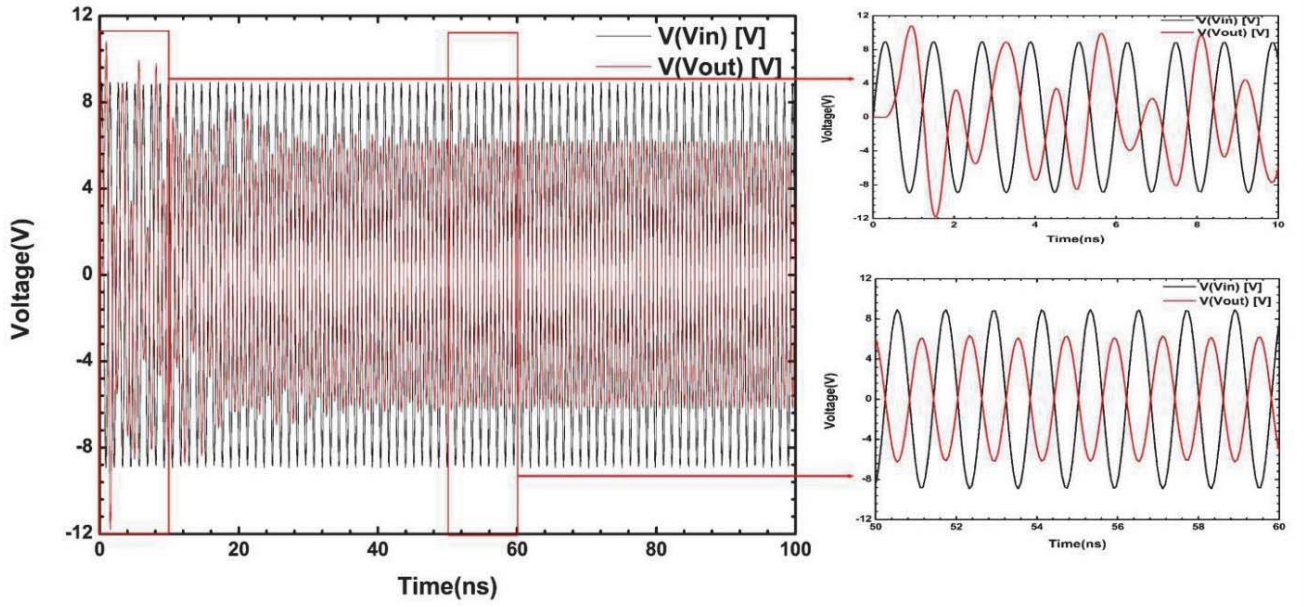

Figure 9. Driver and receive RF signals of the initial design model.

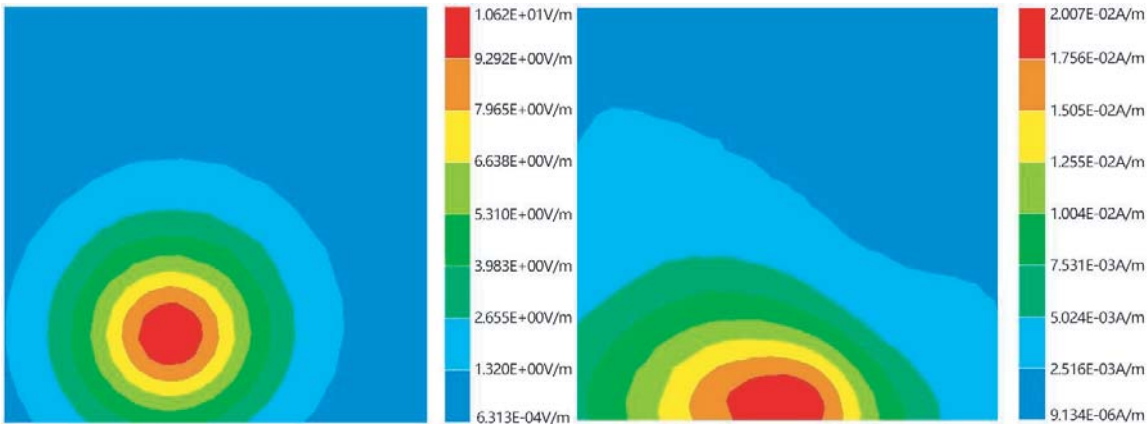

Figure 10. Near-field simulation results of the initial design model at 836 MHz. (a) E-field intensity and (b) H-field intensity.

impedance of the component pads and transmission line, which can effectively improve the signal transmission quality of this discontinuous impedance structure. The via is classified as a capacitive discontinuity because the capacitance exists between the drilled hole and inner layers. Therefore, the radius of the anti-pad is appropriately increased to cancel discontinuous impedance based on the connection structure at both ends of the via.

After the optimized design, the same simulation analysis is conducted to investigate the effect of the optimized design model on electromagnetic radiation. Figure 11 shows the S-parameter simulation results for the optimized design model from 0.1 GHz to 5 GHz. S_{21} increases 0.72 dB, and S_{11} decreases 9.62 dB compared to the initial simulation results of Figure 8, which shows that the optimized design model not only achieves the same function, but also improves the transmission quality of the RF signal.

In addition, from the time-domain simulation results, as shown in Figure 12, the signal amplitude of the receive port is basically the same as the driver port, indicating that the signal has a smaller energy

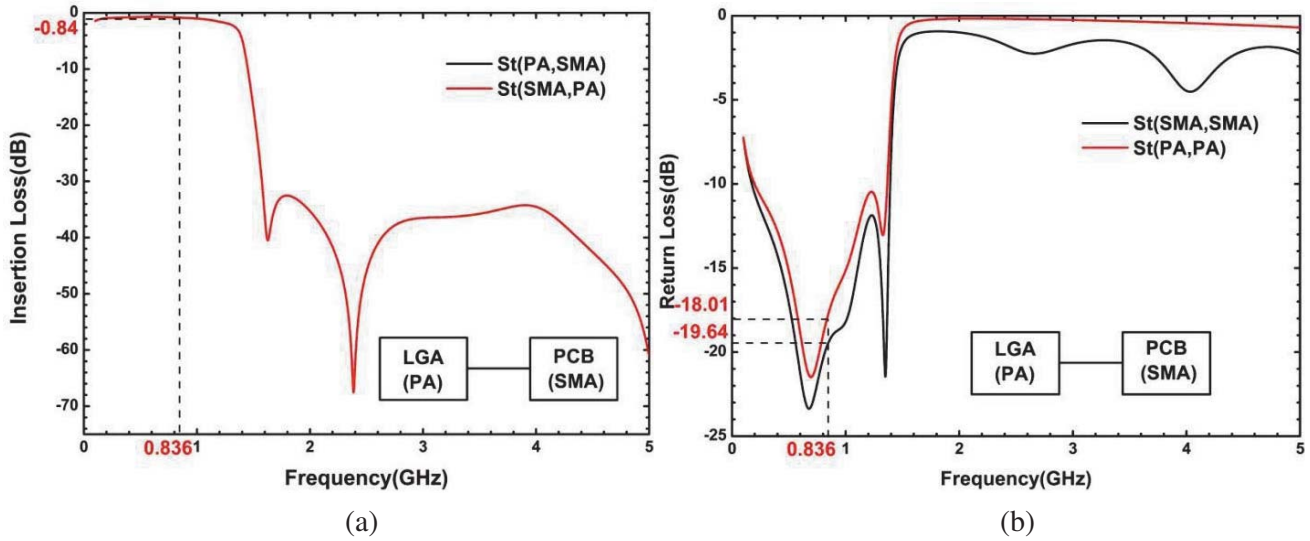

Figure 11. S-parameter simulation results of the optimized design model from 0.1 GHz to 5 GHz. (a) S_{21} and (b) S_{11}.

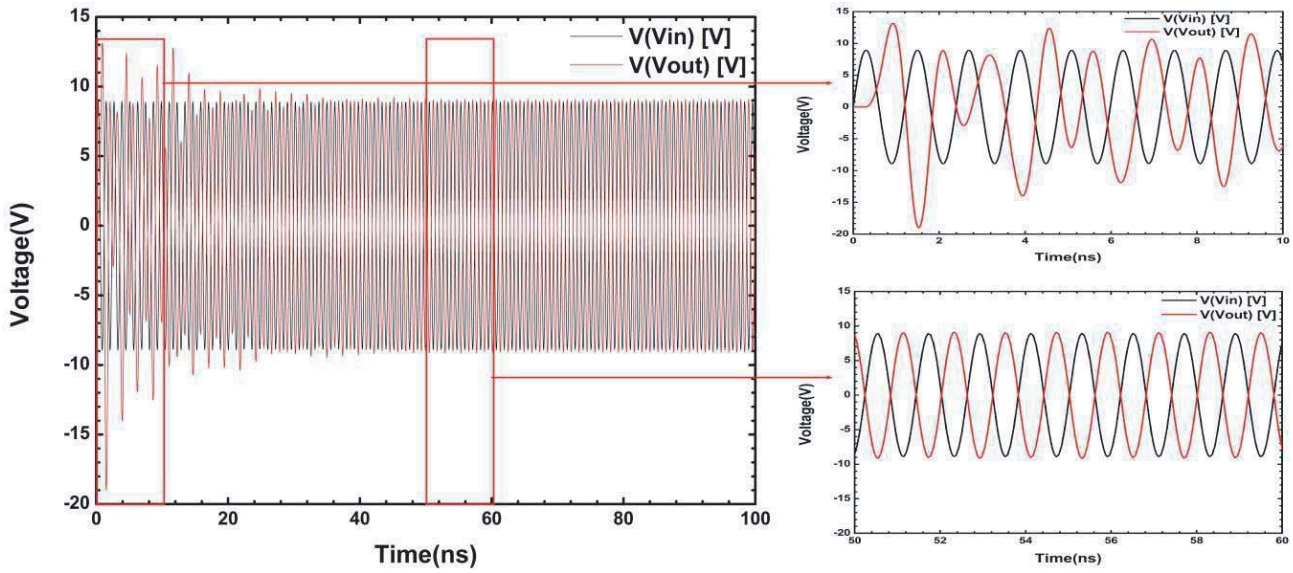

Figure 12. Driver and receive RF signals of the optimized design model.

loss in the process of signal transmission than the initial NB-IoT. Compared with the initial near-field radiation results, the energy distribution of the optimized design model is approximately the same, as shown in Figure 13, but the radiation intensity is decreased, in which the maximum E-field has been suppressed from 1.062E+01 V/m to 6.175E+00 V/m, and the maximum H-field has been restrained from 2.007E-02 A/m to 8.494E-03 A/m.

5. FABRICATION AND NEAR-FIELD RADIATION MEASUREMENT OF OPTIMIZATION DESIGN MODULE

The NB-IoT module and test board are fabricated based on the optimized design model. The manufactured NB-IoT module with a size of 14 mm × 14 mm is mounted on the bottom of the test

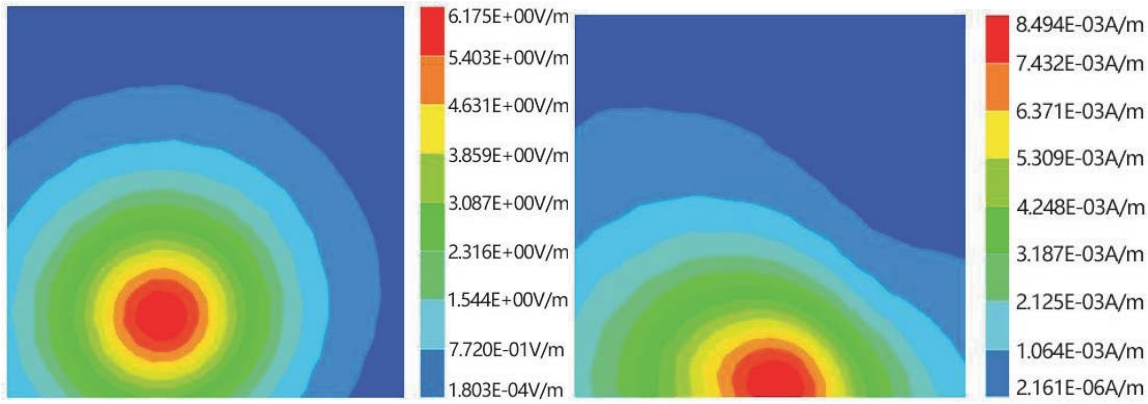

Figure 13. Near-field simulation results of the optimized design model at 836 MHz. (a) E-field intensity and (b) H-field intensity.

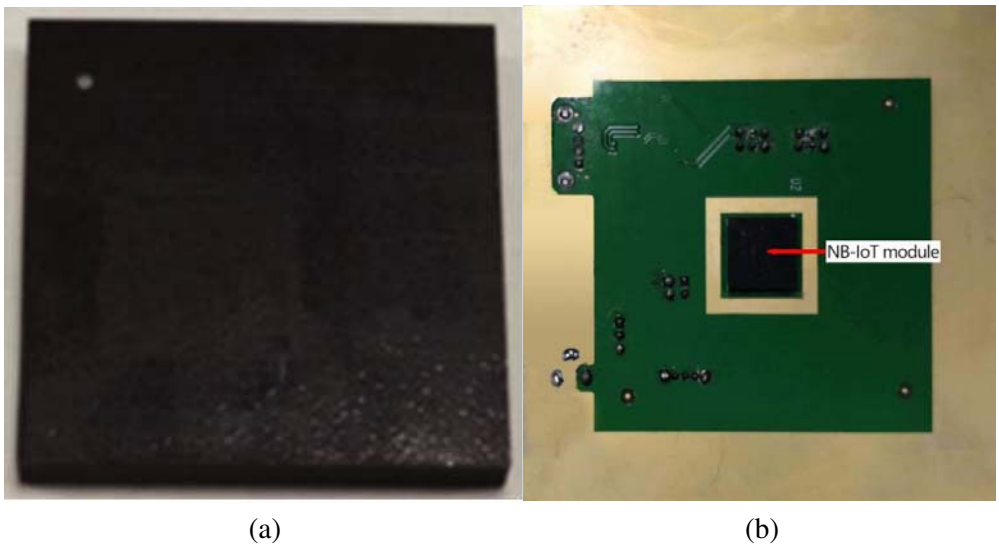

Figure 14. Test sample. (a) NB-IoT module and (b) near-field test board.

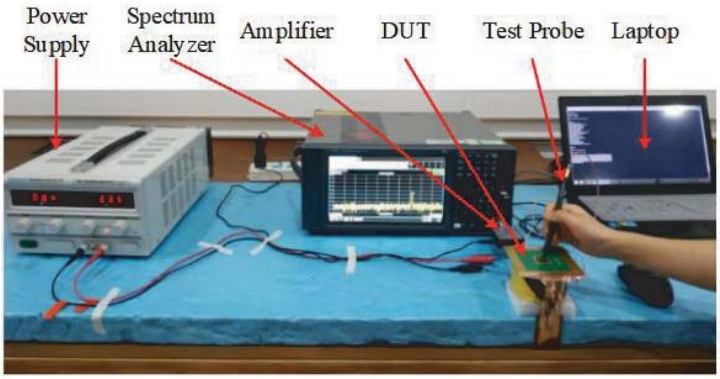

Figure 15. Near-field radiation measurement.

board to make up an overall sample of near-field measurement, as shown in Figure 14.

According to the test standard IEC61967-3 of IC EMC, the surface scanning method is used for the near-field radiation measurement. Figure 15 shows a near-field scanning system. The patterns of the measured E-field and H-field along the Z direction at 836 MHz are shown in Figure 16. The maximums of E-field and H-field intensity are about 6.145 V/m and 0.014 A/m, respectively.

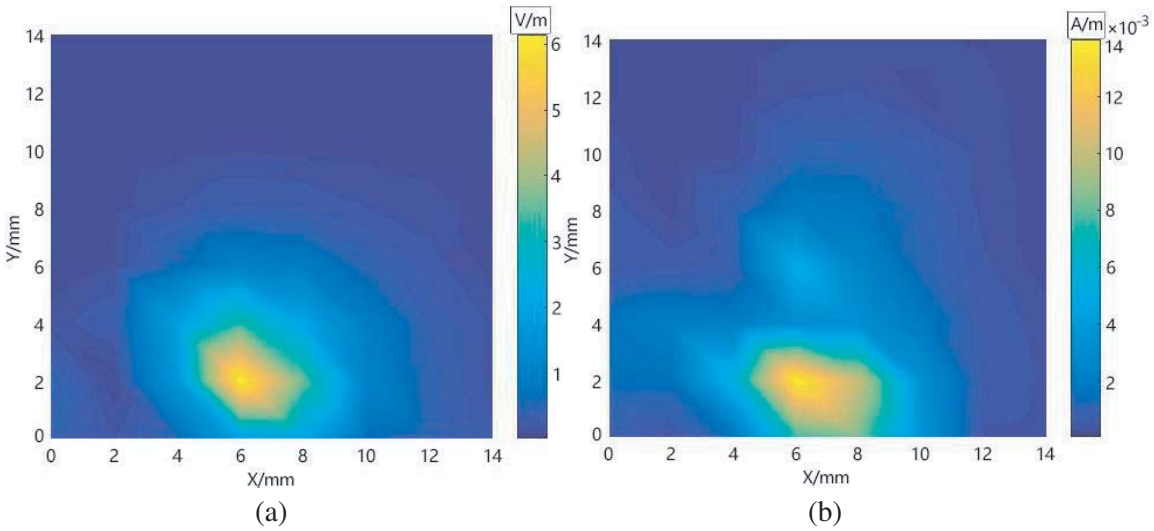

Figure 16. Measured near-field radiation patterns of the NB-IoT module at 836 MHz. (a) E-field intensity and (b) H-field intensity.

A comparison of maximum near-field radiation intensity between simulation and measurement is concluded in Table 1, which demonstrates the effectiveness of the simulation and indicates the optimized module can effectively restrain EMI.

Table 1. Comparison of maximum near-field radiation intensity between simulation and measurement.

NB-IoT module	Max: E-field (V/m)	Max: H-field (A/m)
Simulation	6.175	0.0085
Measurement	6.145	0.014

6. CONCLUSION

In this paper, a package-board co-design method for improving the signal transmission quality is discussed, and the electromagnetic radiation intensities generated by the NB-IoT module before and after the optimized design are quantitatively analyzed. S_{21} increases from -1.56 dB to -0.84 dB, and S_{11} decreases from -8.39 dB to -18.01 dB at 836 MHz. The time-domain results indicate that the RF signal power has been significantly improved. Therefore, it can be concluded that the optimized design restrains the maximum E-field intensity by 41.85% and the maximum H-field intensity by 57.68%. The measurement results of near-field radiation not only effectively verify the correctness of the simulation modeling, but also indicate the feasibility of the optimized co-design method. Our work could be extended to the design of other similar types of packages to restrain an EMI problem of circuit's operating frequency.

ACKNOWLEDGMENT

This research was funded by the National Natural Science Foundation of China, 61974077 and 61804084.

REFERENCES

1. Cunha, T. R., H. M. Teixeira, J. C. Pedro, et al., "Validation by measurements of an IC modeling approach for SiP applications," *IEEE Transactions on Components, Packaging and Manufacturing Technology*, Vol. 1, No. 8, 1214–1225, Aug. 2011.
2. Yoon, S. W., S. Y. L. Lim, A. G. K. Viswanath, S. Thew, T. C. Chai, and V. Kripesh, "Reliability of a silicon stacked module for 3-D SiP microsystem," *IEEE Transactions on Advanced Packaging*, Vol. 31, No. 1, 127–134, Feb. 2008.
3. Liu, L. T., M. Y. Yu, Y. Z. Ye, et al., "Design and simulation of SIP for RF system," *2005 6th International Conference on Electronic Packaging Technology*, 102–104, 2005.
4. Kripesh, V., S. W. Yoon, V. P. Ganesh, et al., "Three-dimensional system-in-package using stacked silicon platform technology," *IEEE Transactions on Advanced Packaging*, Vol. 28, No. 3, 377–386, Aug. 2005.
5. Kelander, I., M. Uusimaki, and A. N. Arslan, "EMC analysis on stacked packages," *2006 17th International Zurich Symposium on Electromagnetic Compatibility*, 602–605, 2006.
6. Jiang, F., M. Li, and L. Gao, "Research on conformal EMI shielding Cu/Ni layers on package," *2014 15th International Conference on Electronic Packaging Technology*, 227–230, 2014.
7. Tsai, M., R. Chiu, D. Huang, et al., "Innovative packaging solutions of 3D double side molding with system in package for IoT and 5G application," *2019 IEEE 69th Electronic Components and Technology Conference (ECTC)*, 700–706, 2019.
8. Liao, K. H., S. C. Hsien, H. H. Wen, et al., "Novel EMI shielding methodology on highly integration SiP module," *2012 2nd IEEE CPMT Symposium Japan*, 1–4, 2012.
9. Hwang, L. T. and T. S. J. Horng, "State-of-the-art IC packages, modules, and substrates," *3D IC and RF SiPs: Advanced Stacking and Planar Solutions for 5G Mobility*, 111–137, IEEE, 2017.
10. Huang, C., C. Hsiao, C. Wang, et al., "Conformal shielding investigation for SiP modules," *2010 IEEE Electrical Design of Advanced Package & Systems Symposium*, 1–4, 2010.
11. Karim, N., J. K. Mao, and J. Fan, "Improving electromagnetic compatibility performance of packages and SiP modules using a conformal shielding solution," *2010 Asia-Pacific International Symposium on Electromagnetic Compatibility*, 56–59, 2010.
12. Fee, T. M., L. S. Kah, G. S. Lock, et al., "Adhesion enhancement for electroless plating on mold compound for EMI shielding with industrial test compliance," *2014 IEEE International Conference on Semiconductor Electronics (ICSE2014)*, 313–316, 2014.
13. Wang, L. B., K. Y. See, J. W. Zhang, et al., "Ultrathin and flexible screen-printed metasurfaces for EMI shielding applications," *IEEE Transactions on Electromagnetic Compatibility*, Vol. 53, No. 3, 700–705, Aug. 2011.
14. He, Y., J. Li, G. Tian, et al., "Study on a conformal shielding structure with conductive adhesive coated on molding compound in 3-D packages," *IEEE Transactions on Electromagnetic Compatibility*, Vol. 58, No. 2, 442–447, Apr. 2016.
15. Hoang, J. V., R. Darveaux, T. Lobianco, et al., "Breakthrough packaging level shielding techniques and EMI effectiveness modeling and characterization," *2016 IEEE 66th Electronic Components and Technology Conference (ECTC)*, 1290–1296, 2016.
16. Wu, T. L., W. S. Jou, S. G. Dai, et al., "Effective electromagnetic shielding of plastic packaging in low-cost optical transceiver modules," *Journal of Lightwave Technology*, Vol. 21, No. 6, 1536–1543, Jun. 2003.
17. Tai, M. F., S. L. Kok, and K. Mukai, "EMI shielding performance by metal plating on mold compound," *2016 IEEE 37th International Electronics Manufacturing Technology (IEMT) & 18th Electronics Materials and Packaging (EMAP) Conference*, 1–4, 2016.

18. Jin, L., H. Y. Zhang, L. Ping, et al., "The electromagnetic shielding effectiveness of a low-cost and transparent stainless steel fiber/silicone resin composite," *IEEE Transactions on Electromagnetic Compatibility*, Vol. 56, No. 2, 328–334, Apr. 2014.
19. Rathi, V. and V. Panwar, "Electromagnetic interference shielding analysis of conducting composites in near- and far-field region," *IEEE Transactions on Electromagnetic Compatibility*, Vol. 60, No. 6, 1795–1801, Dec. 2018.
20. Hsiao, C. Y., C. H. Huang, C. D. Wang, et al., "Mold-based compartment shielding to mitigate the intra-system coupled noise on SiP modules," *2011 IEEE International Symposium on Electromagnetic Compatibility*, 341–344, 2011.
21. Sitaraman, S., J. Min, M. R. Pulugurtha, et al., "Modeling, design and demonstration of integrated electromagnetic shielding for miniaturized RF SOP glass packages," *2015 IEEE 65th Electronic Components and Technology Conference (ECTC)*, 1956–1960, 2015.
22. Huang, S. and J. DeLaCruz, "Improvements of system-in-package integration and electrical performance using BVA wire bonding," *IEEE Transactions on Components, Packaging and Manufacturing Technology*, Vol. 7, No. 7, 1020–1034, Jul. 2017.
23. Huang, S. and J. DeLaCruz, "Techniques for improving system-in-package integration and electrical performance," *2017 IEEE International Symposium on Electromagnetic Compatibility & Signal/Power Integrity (EMCSI)*, 129–134, 2017.
24. Huang, S., X. Ye, N. Kang, et al., "Suppression of couplings in high-speed interconnects using absorbing materials," *IEEE Transactions on Electromagnetic Compatibility*, Vol. 58, No. 5, 1432–1439, Oct. 2016.
25. Pulici, P., G. P. Vanalli, M. A. Dellutri, et al., "Signal integrity flow for system-in-package and package-on-package devices," *Proceedings of the IEEE*, Vol. 97, No. 1, 84–95, Jan. 2009.
26. Jandhyala, V., D. Gope, S. Chakraborty, et al., "Toward building full-system EMI verification and early design flows through full-wave electromagnetic simulation," *International Journal of RF and Microwave Computer-Aided Engineering*, Vol. 22, No. 1, 104–115, Jan. 2012.
27. Song, T., C. Liu, Y. Pen, et al., "Full-chip signal integrity analysis and optimization of 3-D ICs," *IEEE Transactions on Very Large Scale Integration (VLSI) Systems*, Vol. 24, No. 5, 1636–1648, May 2016.
28. Oikawa, R., "Package substrate built-in three-dimensional distributed matching circuit for high-speed SerDes applications," *2008 58th Electronic Components and Technology Conference*, 676–682, 2008.
29. Seo, D., H. Lee, M. Park, et al., "Enhancement of differential signal integrity by employing a novel face via structure," *IEEE Transactions on Electromagnetic Compatibility*, Vol. 60, No. 1, 26–33, Feb. 2018.
30. Chuang, H. H., W. D. Guo, Y. H. Lin, et al., "Signal/Power integrity modeling of high-speed memory modules using chip-package-board coanalysis," *IEEE Transactions on Electromagnetic Compatibility*, Vol. 52, No. 2, 381–391, May 2010.